Nanoscale

Accepted Manuscript

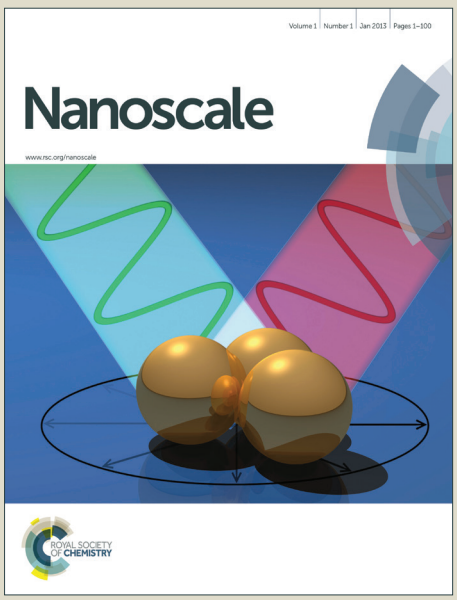

ROYAL SOCIETY OF CHEMISTRY

www.rsc.org/nanoscale

Utilizing the protein corona around silica nanoparticles for dual drug loading and release

Shakiba Shahabi [a], Laura Treccani [a, *], Ralf Dringen [b], Kurosch Rezwan [a, c]

[a] Advanced Ceramics, University of Bremen, Am Biologischen Garten 2, 28359 Bremen, Germany
[b] Centre for Biomolecular Interactions Bremen and Centre for Environmental Research and Sustainable Technology, Faculty 2 (Biology/Chemistry), University of Bremen, Leobener Strasse, NW2, 28359 Bremen, Germany
[c] MAPEX Center for Materials and Processes, University of Bremen, Germany

**Corresponding author:*
Dr. Laura Treccani
Advanced Ceramics, University of Bremen, Am Biologischen Garten 2, 28359 Bremen, Germany
E-Mail: treccani@uni-bremen.de
Tel: +49 421 218 64938
Fax: +49 421 218 64932

Abstract

A protein corona forms spontaneously around silica nanoparticles (SNPs) in serum-containing media. To test whether this protein corona can be utilized for loading and release of anticancer drugs we incorporated the hydrophilic doxorubicin, the hydrophobic meloxicam as well as their combination in the corona around SNPs. Application of corona-covered SNPs to osteosarcoma cells revealed that drug-free particles did not affect the cell viability. In contrast, SNPs carrying a protein corona with doxorubicin or meloxicam lowered cell proliferation in a concentration-dependent manner. In addition, these particles had even a stronger antiproliferative potential than the respective concentrations of free drugs. Best antiproliferative effects were observed for SNPs containing both doxorubicin and meloxicam in their corona. Co-localization studies revealed the presence of doxorubicin fluorescence in nucleus and lysosomes of cells exposed to doxorubicin-containing coated SNPs, suggesting that endocytotic uptake of the SNPs facilitates the cellular accumulation of the drug. Our data demonstrate that the protein corona, which spontaneously forms around nanoparticles, can be efficiently exploited for loading the particles with multiple drugs for therapeutical purposes. As drugs are efficiently released from such particles they may have a high potential for nanomedical applications.

Key Words:

Doxorubicin, Drug delivery, Osteosarcoma, Protein corona, Silica nanoparticle

Introduction

When nanoparticles (NPs) are introduced into biological systems, they firstly encounter physiological fluids, which are complex mixtures of hundreds of distinct proteins.[1, 2] For serum-containing solutions is well known that serum proteins can rapidly and non-specifically adsorb onto the NP surface which leads to the formation of a so-called "protein corona".[3] Under physiological conditions, the protein corona masks the NP surface and, therefore, considerably alters NP surface properties and behaviors.[2, 4]

The formation of a protein corona is in general considered as a negative and unavoidable side effect due to its unpredictability, complexity and possible undesirable biological implications.[5] However, recent studies have reported promising advantages of the protein corona. For instance, adsorbed proteins on the NP surface can increase the colloidal stability,[6-9] facilitate the cellular internalization of NPs,[10] reduce the cytotoxic effects of bulk particles,[11] enhance specific targeting,[12] and potentially eliminate undesired immune responses to the drug carrier.[13] Recent investigations have also shown that a multilayered protein corona around gold NPs can be strategically employed as "sponge" to be loaded with drugs at high payload capacities and with enhanced carrier properties.[14, 15] Indeed, as proteins have both hydrophilic and hydrophobic groups, they can bind and host both hydrophilic and hydrophobic drugs.[16] Therefore, the protein corona of NPs has the potential to be used as smart carrier for delivering chemotherapeutics and anti-cancer drugs with limited high-dose toxic effects. In addition, incorporation of drugs into the protein corona avoids drawbacks like intermolecular repulsion or steric hindrances which are associated with the covalent coupling of drugs to NP.[15]

In our study, we utilize the protein corona associated with SNPs as a versatile nanocarrier for encapsulation of single or dual therapeutics. A similar concept to show the possibility of drugs or DNA incorporation in the corona around gold nanorods is introduced by Kah et al.[14] Here, as core substrate for the generation of a protein corona, silica NPs (SNPs) were synthesized via an amino acid catalyzed seed regrowth technique (ACSRT),[17] as illustrated in Scheme 1a. SNPs feature several advantages like high chemical stability, biocompatibility,[18] optical transparency,[19] aqueous dispersibility,[20] versatile surface functionalization and bio-conjugation.[21, 22] Protein coronas on SNPs were formed by incubating SNPs with fetal calf serum (FCS), a commonly used growth supplement for cell culture media. Simultaneously with the serum the hydrophilic anti-cancer drug doxorubicin (Dox) and/or the hydrophobic drug meloxicam (Mel) were applied to the SNPs to load the forming protein

corona with the drugs (Scheme 1b). Dox and Mel were selected because of their therapeutical relevance for osteosarcoma bone tumor treatment.[23, 24] As it has been reported that a combination of Dox and Mel synergistically enhanced anti-cancer effects,[25, 26] we prepared in addition to the single drug loaded SNPs (SNP//corona+Dox and SNP//corona+Mel) also particles containing both drugs (SNP//corona+Dox+Mel). To examine the effect of varying drugs concentration in the corona, different types of drug loaded SNP//corona (A, B or C) were prepared by applying three different amounts of the respective therapeutics (Table 1).

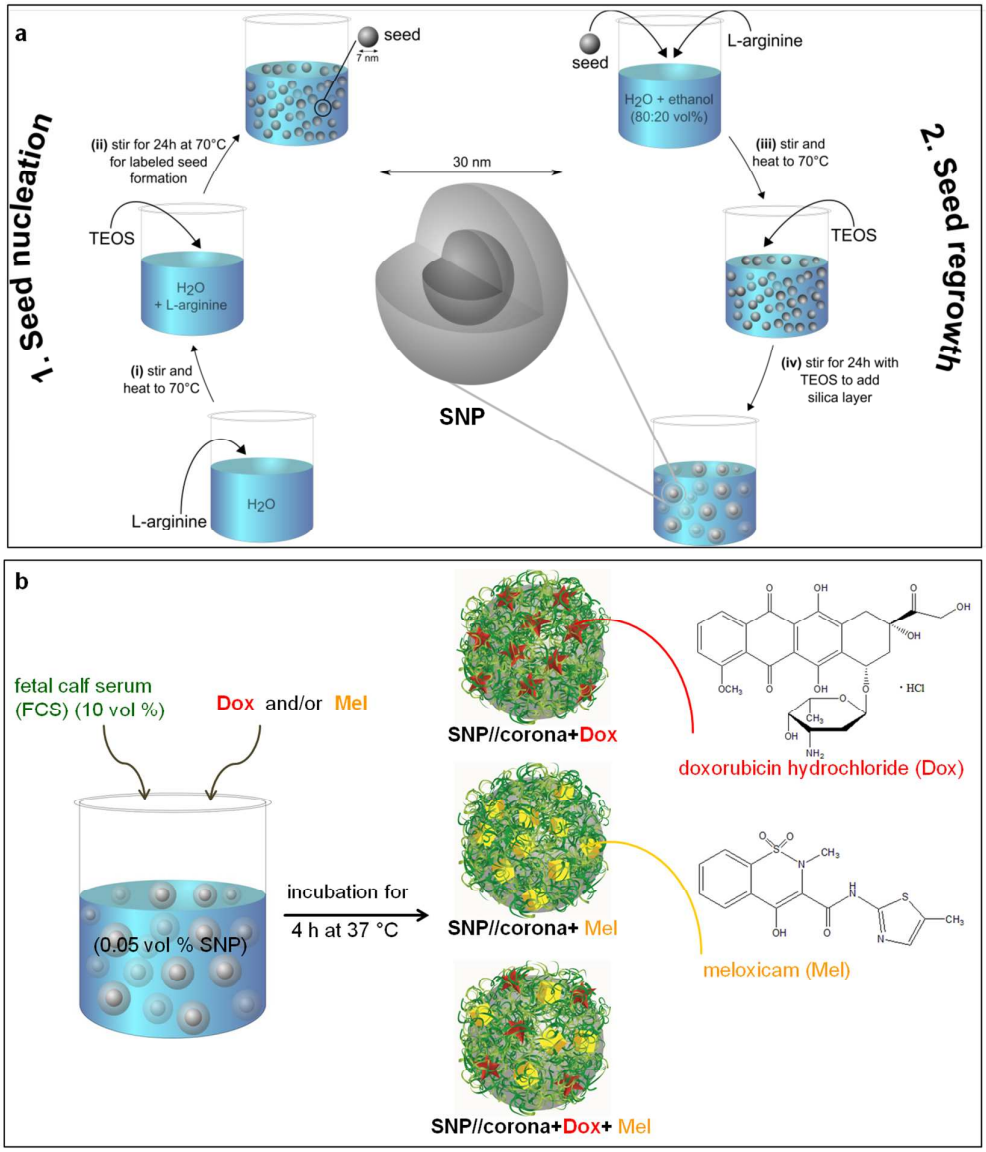

Scheme 1. Schematic illustration of the SNP synthesis via ACSRT (a) and the preparation of SNP//corona and its simultaneous loading with Dox, Mel or Dox+Mel (b).

Table 1. Nomenclature, drug concentration code and amount of drugs (µmol) used for loading the corona per 1 ml of SNP dispersion (0.05 vol %).

nomenclature	drug concentration code	Dox [µmol]	Mel [µmol]
SNP (silica NP)	---	---	---
FSNP (fluorescence silica NP)	---	---	---
SNP//corona	---	---	---
FSNP//corona	---	---	---
SNP//corona+Dox A	A	0.0431	---
SNP//corona+Dox B	B	0.0862	---
SNP//corona+Dox C	C	0.1293	---
SNP//corona+Mel A	A	---	1.6669
SNP//corona+Mel B	B	---	3.3338
SNP//corona+Mel C	C	---	5.007
SNP//corona+Dox A+Mel A	A	0.0431	1.6669

For our study, we investigated first for both drugs and their combination the loading in and the release from SNP//corona. Subsequently, the drug-containing particles were applied to human osteosarcoma cells (MG-63) and their antiproliferative potential were compared to that of the free drugs. Cellular uptake of drug-free nanocarrier (SNP//corona) was confirmed by using corona-conjugated fluorescent labeled silica NP (FSNP//corona) with physicochemical properties similar to SNP//corona. Furthermore, intracellular localization of drug-loaded SNP//corona and free drugs were studied using the fluorescence microscopy.

2. Experimental Section

2.1. Chemicals

For particle synthesis, corona formation and drugs loading, tetraethyl orthosilicate (TEOS, >99%, lot no. BCBK1670V), L-arginine (>98%, lot no. MKBH2770V), rhodamine B isothiocyanate (RBITC, mixed isomers, lot no. MKBJ9031V), absolute ethanol (>98%, lot no. SZBB1570V), feta calf serum (FCS, lot no. 010M3395) doxorubicin hydrochloride (Dox, lot no. SLBH4977V) and meloxicam (Mel, Id. 0092V2) were purchased from Sigma Aldrich (Germany).

Cell culture experiments were carried out on human osteosarcoma cells (MG-63, passage 98, lot no. 2006399, ATCC, Germany). Dulbecco/Vogt modified Eagle's minimal essential medium (D-MEM, high glucose, lot no. 1206393), antibiotic–antimycotic solution (lot no. 1209917), Alexa Fluor®488 phalloidin (AF488, 2 U/ml, lot no. 1151587) and LysoTracker® (DND-22, lot no. 791512) were from Invitrogen (Germany). Fetal calf serum (FCS, lot no. 010M3395), paraformaldehyde (PFA, lot no. 53260),

phosphate buffered saline (PBS, lot no. SLBF5741V), Triton™ X-100 (lot no. MKBL5839V), sodium chloride (NaCl, lot no. 038K00451) and 4',6-diamidino-2-phenylindole (DAPI, 0.5 µg/ml, lot no. 1242642) were supplied by Sigma-Aldrich (Germany). The cell proliferation assay WST-1 (lot no. 14310400, Roche Diagnostics, Germany) and the lactate dehydrogenase LDH Pierce™ assay (lot no. OL17881450, Thermo Scientific, Germany) were purchased from the suppliers as specified. Double deionized water (ddH_2O) with a conductivity <0.4 µS cm^{-1} was obtained from an ultrapure water system (Synergy, Millipore, USA) and used for all experiments.

2.2. Preparation of SNPs and FSNPs

The synthesis of SNPs and FSNPs based on the amino acid catalyzed seed regrowth technique (ACSRT) [17] are schematically illustrated in **Scheme 1a**, respectively. For SNP, 17.4 mg L-arginine were first dissolved in 16.9 ml ddH_2O (final concentration 0.006 M). The L-arginine solution was stirred thoroughly at room temperature for 10 min and then heated up to 70 °C before TEOS addition. The mixture was heated in an oil bath at 70 °C under magnetic stirring at 400 rpm for 24 h. During this time silica seeds formed and this silica seed suspension was used as stock for the following regrowth step. To regrow the seeds to a desired size of 30 nm, first L-arginine was dissolved in a mixture of water and ethanol (volume ratio of 1:4) at room temperature. Subsequently, 2 ml of silica seed suspension were added to the L-arginine solution and the mixture was stirred for 10 min before heating up to 70 °C. Thereafter, 0.5 ml TEOS were added and the suspension was constantly stirred at 400 rpm and kept at 70 °C for 24 h.

FSNPs were synthesized using a similar procedure. First RBITC was dissolved in water (concentration 0.01 M) and added to the L-arginine solution. The molar composition of the reactants was adjusted to 1: 0.02: 0.001 of TEOS: L-arginine: RBITC. The other reaction parameters (pH, temperature, stirring rate, time, L-arginine concentration, volume and ratio of water/ethanol, as well as seed/TEOS proportion) remained unaltered. This enabled the synthesis of FSNPs with the size comparable to SNPs.

2.3. Simultaneous formation of protein corona and drug loading

SNP (0.05 vol %) were dispersed in DMEM and deagglomerated using an ultrasound horn (Sonifier 450, Branson, Germany) at the frequency of 20 kHz, with two ultrasound pulses of 150 W/s for 30 min. FCS (10 vol %) and drugs (Dox or Mel) or their combination (Dox+Mel) were added in the

concentrations indicated (**Table 1**) simultaneously to the prepared SNP dispersion and incubated at 37 °C for 4 h (**Scheme 1b**). Afterwards, the dispersion of SNP with serum proteins and drugs was centrifuged (2,000 g for 5 min) and washed with DMEM to remove excess of proteins and unbound drugs. After this, the SNPs were resuspended in DMEM. As controls, SNP//corona and FSNP//corona were prepared with the same procedure but without loading any drugs.

For single drug loaded nanocarrier (SNP//corona+Dox or SNP//corona+Mel), three samples with three different initial amounts of drugs were prepared. Sample names and corresponding drug concentration codes (A, B or C) are described in **Table 1**. Furthermore, for dual drug loaded nanocarrier, the sample SNP//corona+Dox A+Mel A was prepared (**Table 1**).

2.4. Particle and corona characterization

UV-Vis absorbance spectra of SNP and SNP//corona without and with drug payloads were obtained using a multiscan GO spectrophotometer (Thermo Scientific, Finland).

Hydrodynamic diameter (D_H) and surface charge of SNP, SNP//corona, FSNP, FSNP//corona and SNP//corona+drugs dispersions ($5{\cdot}10^{-4}$ vol %) in DMEM were measured using dynamic light scattering (DLS) and zeta potential (Malvern Zetasizer, UK). The averages and standard deviations of zeta potential data from three independent measurements are given.

Transmission electron microscopy (TEM) images were recorded using a Titan 80-300 ST microscope (FEI^{TM}, Eindhoven, the Netherlands). SNPs and FSNPs were deposited onto a carbon-coated copper grid (PLANO GmbH, Wetzlar, Germany) and carefully shaking to leave only a small deposit.

2.5. Determination of drug loading efficiency (L.E.) and release

2.5.1. Generation of standard curves

Standard curves of Dox or Mel were generated by dissolving different amounts of these compounds in the supernatant obtained after twice centrifugation of the SNP//corona dispersion in DMEM at 2,000 g for 5 min. The fluorescence emission intensities of the Dox-solutions were recorded (λ_{ex}: 485 nm, λ_{em}: 590 nm) using a microplate reader (Plate Chameleon II model 425-155, Hidex, Finland) and used for drawing the standard curves. Absorption spectra of both Dox- and Mel-solutions were measured at 365 nm, the characteristic wavelength of Mel, with the multiscan GO spectrophotometer (Thermo Scientific, Finland) and were used for generation of the standard curves. For each drug, two standard

curves were obtained at pH 4.8 and 7.4 as release studies were performed at these pH values as described below. The acidic pH value was established by adjusting the pH with HCl.

2.5.2. Measurement of the loading efficiency for drugs in the protein corona

Loading efficiency (L.E.) for each drug was measured by drug depletion, calculated as the ratio between the amount of the drug content in the SNP protein corona and the initial amount of the drug used for the loading. The amount of loaded drugs was quantified indirectly by spectrometrically measuring the concentration of residual unbound drugs in the supernatant by using respective standard curves. The concentration of the unloaded Dox in the supernatant of each SNP//corona+Dox was determined by fluorimetry (λ_{ex}: 485 nm, λ_{em}: 590 nm). Similarly, the amount of the unloaded Mel in SNP//corona+Mel was quantified by measuring the absorbance at 365 nm. To determine the L.E. in the dual drug loaded nanocarrier (SNP//corona+Dox+Mel), it was necessary to quantitatively determine the amount of both drugs in the supernatant. Thus, firstly, the amount of unloaded Dox was measured based on the fluorescence measurements. Secondly, to quantify the concentration of Mel, total light absorption at 365 nm from both Dox and Mel was measured. The absorbance generated only from Mel was calculated by subtracting the absorbance of Dox from the total absorbance value. All measurements were performed in triplicates.

2.5.3. Drugs release measurements

For drug release measurements, dispersions of SNP//corona+Dox, SNP//corona+Mel or SNP//corona+Dox+Mel in DMEM were incubated at 37 °C for up to 168 h at pH 7.4 or pH 4.8. pH 4.8 was set by adding HCl. The pH of all samples was maintained during the incubation by monitoring the pH every 12 h and by adding, if required, additional HCl to compensate for a slight increase in pH. The samples were permanently shaken using a horizontal shaker (Unimax 1011, Heidolph Instruments, Germany). After the given time intervals, the samples were collected and centrifuged twice at 2,000 g for 5 min. The supernatants were collected and used for spectral analysis. The amounts of Dox or Mel released from the particles into the supernatants were determined as above described (section 2.5.2) and are given as percentage of the initial amount that had been loaded into the corona. Release data are given as averages and standard deviations of triplicate measurements.

2.5.4. Proteins adsorption and release measurement

The concentration of adsorbed and unbound serum proteins in the supernatant of each SNP//corona+drug was determined via the solution-depletion method using the Pierce® BCA protein assay (lot no. OD 187710, Thermo Scientific, Germany), as described in the supplier's instructions. The amount of adsorbed proteins was calculated indirectly as difference between the initially applied concentration of protein and that determined in the supernatant of the particles. For release experiments the amount of serum proteins in the supernatant after a given incubation time (1, 4 or 7 d) was quantified using the same assay. The three time points were selected to allow comparison to the respective conditions of cell experiments. All measurements were performed in triplicates.

2.6. Cell culture experiments

2.6.1 Cell culturing

In vitro tests were performed with MG-63 cells as described previously in Holthaus et al..[27] Briefly, the cells were cultured in DMEM supplemented with 10% heat-inactivated FCS and 1% antibiotic-antimycotic solution in a cell incubator (C200, Labotect Labor-Technik-Göttingen, Germany) at 37 °C with 10% CO_2 and 95% relative humidity (RH). Cells were cultured in cell culture flasks (75 cm^2, NUNC, Fischer Scientific, Germany) for up for one week and the medium was refreshed every 2 days. Cells were trypsinized and seeded at a density of $2.5 \cdot 10^4$ cells/ml medium onto 15 mmØ Thermanox® coverslips (NUNC) placed in wells of a 24-well polystyrene multidish (NUNC) and incubated at 37 °C with 10% CO_2 and 95% RH overnight. Dispersions of SNP//corona, FSNP//corona or SNP//corona+drugs were added to the cell medium to obtain a final particle concentration of 100 µg/ml. As drug controls, the equivalent concentrations of free Dox, Mel or Dox+Mel as present in the corona of the respective particles were added to the cells. As negative control, MG-63 cells with the same initial seeding density were incubated in the absence of particles or drugs.

2.6.2 Determination of cell proliferation and cell viability

The cell proliferation was evaluated using the WST-1 assay. After each sampling time (1, 4 or 7 d), 100 µl cell proliferation reagent of WST-1 were added to the culture wells and the cells were incubated at 37 °C with 10% CO_2 and 95% RH for 2 h. Thereafter, the cell medium was harvested and centrifuged for 5 min at 12,000 g to remove the particles. Formazan produced and released by living cells was quantified spectrometrically using the multiscan GO spectrophotometer at 450 nm with a

reference wavelength of 650 nm. An identical volume of the culture medium and reagent WST-1 which had not been into contact with the cells was used in the experiments as a blank.

The cellular and extracellular activity of the cytosolic enzyme LDH was quantified using the Pierce™ assay according to supplier´s instructions. After each sampling time, the media were collected from each well and centrifuged at 12,000 g for 5 min to remove the particles before measurement of extracellular LDH. For quantification of cellular LDH, the cells were rinsed with PBS buffer (0.01 M phosphate buffer pH 7.4, containing 0.0027 M potassium chloride and 0.137 M sodium chloride in ddH_2O), detached with trypsin/EDTA solution and centrifuged at 600 g for 10 min to separate the cell pellet from the supernatant. Afterwards the lysis buffer (1% Triton™ X-100 in 0.9% NaCl) was added to the cell pellets and mixed till a clear solution was obtained. 50 µL cell media or cell lysates were used for the LDH assay and the absorbance was measured at 490 nm with a reference wavelength of 680 nm using the multiscan GO spectrophotometer. The LDH release is an indicator for damaged cells and the amount of extracellular LDH activity is given as percent of the total LDH activity per well (medium plus lysate).

2.6.3 Cell staining and imaging

After incubation for 1, 4 or 7 d, MG-63 cells were rinsed twice with PBS buffer and fixed for 15 min at room temperature with 4 % PFA. Cell nuclei and actin cytoskeleton were fluorescently stained with DAPI and with AF488, respectively. Fluorescence microscope micrographs were taken with an AX-10 fluorescence microscope (Carl Zeiss, Germany) using three fluorescence channels: FS02 (λ_{ex}: 300-400 nm, λ_{em}: > 420 nm) for DAPI and LysoTracker®, FS09 (λ_{ex}: 450-490 nm, λ_{em}: > 515 nm) for AF488 and FS15 (λ_{ex}: 535-558 nm, λ_{em}: > 590 nm) for RBITC and Dox. Particle uptake and distribution within the cells were analysed using fluorescent FSNP//corona. As Dox showed an intense red fluorescence, it was possible to study the cellular uptake of Dox loaded SNP//corona as well as of free Dox using fluorescence microscopy. Cellular localization of particles or drugs within lysosomes was investigated by co-incubation with the fluorescent dye LysoTracker®. To avoid possible autofluorescence of Thermanox® coverslips in the lysosomal co-localization experiments, MG-63 cells were cultured on glass coverslips (lot. no. 0983, VWR, Germany) and incubated with SNP//corona, FSNP//corona, SNP//corona+drugs or free drugs for 1, 4 or 7 d. Afterwards cells were incubated with LysoTracker® (75 nM) for 1 h, then washed twice with PBS and fixed with PFA. Cell actin cytoskeleton was stained with AF488 as previously described.[27] The applied LysoTracker® is a blue fluorescent dye that stains

the acidic lysosomes. Hence, cellular co-localization of the FSNP//corona, Dox loaded SNP//corona or free Dox (all with red fluorescence) with LysoTracker® will yield a magenta overlap in the merged images.

2.6.4 Determination of cellular Dox uptake

The amount of Dox uptake in cells was quatified by fluorimetry. For the quantitative determination of Dox uptake in cells, fluorimetry was used. Dox internalization in MG-63 cells was evaluated in the microplate reader (Plate Chameleon II model 425-155, Hidex, Finland) as described in Meng et al..[28] MG-63 cells ($5 \cdot 10^3$ cells in 0.2 ml medium) were placed into wells of a black 96-well plate (Greiner, Germany). Subsequently, the cells were treated with SNP//corona+Dox, SNP//corona+Dox+Mel (100 µg/ml), free Dox or free Dox+Mel at the same concentrations as applied by drug-loaded SNPs for 1, 4 or 7 d. After washing the cells twice with cold PBS, the intracellular Dox fluorescence was measured (λ_{ex}: 485 nm, λ_{em}: 590 nm). Dox fluorescence in cells after different incubation periods was recorded and control cells (treated without any drug or particle treatment) were used as a blank.

To quantify the nuclear Dox fluorescence intensity, the Carl Zeiss Zen software was used to analyse the fluorescence microscopy images of the cells captured at the end of each sampling point (day 1, 4 or 7). The signal intensity of the red channel (reflecting Dox internalization in 20 separate nuclei) was determined after application of SNP//corona+Dox, SNP//corona+Dox+Mel, free Dox or free Dox+Mel.

2.6.5 Statistical analysis

Quantitative data (zeta potential, drugs L.E. and release, adsorbed and released proteins, cell viability, LDH activity, intracellular Dox fluorescence) are given as mean ± standard deviation of values obtained in three independently performed experiments. The statistical analysis was performed using the software Minitab 16 (Minitab Inc., Pennsylvania). The data were subjected to one-way analysis of variance (ANOVA) followed by Dunnett's method for multiple comparisons. *p*-values below 0.05 ($p<0.05$) were considered to be statistically significant.

3. Results

SNPs were synthesized via ACSRT and subsequently used for corona formation experiments with FCS in the absence or presence of Dox and/or Mel. TEM analysis showed that both the synthesized SNP and FSNP were spherical, monodisperse and had a mean diameter of 30 nm (Figure S1a, b). In

addition, SNP, SNP//corona and drug loaded SNP//corona were analyzed by UV-Vis spectrophotometry (Figure S2). Compared to uncovered SNPs, the absorption spectra of SNP//corona and SNP//corona+drugs showed a more narrowed peak in the absorption range between 200 and 240 nm and a blue-shifted of about 10 nm. All drug loaded SNP//corona showed a similar absorption behavior as the blank unloaded nanocarrier (SNP//corona), suggesting that the presence of drugs does not affect nor disturb the corona formation.

The difference between surface charges of uncovered particles (SNP or FSNP) and corona-covered particles (SNP//corona or FSNP//corona) was assessed by zeta potential measurements carried out in DMEM (Figure 1a). The zeta potential values of uncovered SNP and FSNP in DMEM were -22 and -20 mV, respectively. A lower surface charge was found after protein corona formation (~ -12 mV) and drug loading (between -10 and -13 mV). The almost identical zeta potentials of all drug-loaded SNP//corona (Figure 1c and Figure S3a, c) suggest that all particles had similar surface charge and that this parameter was not affected by the type nor by the concentration of the loaded drugs.

DLS size analysis of SNP and FSNP, without protein corona, showed a similar narrow size distribution of these particles (Figure 1b). A slight increase of the average hydrodynamic diameter (D_H) was observed in both SNP and FSNP which contained a protein corona (Figure 1b). All types of the drug loaded SNP//corona were also characterized using DLS (Figure 1d and Figure S3b, d), revealing that the D_H of SNP//corona+Dox for the three different Dox concentrations loaded were similar as that of unloaded SNP//corona (Figure 1b, d and Figure S3b). In contrast, SNP//corona+Mel and SNP//corona+Dox+Mel had a higher D_H compared to drug-free SNP//corona (Figure 1b, d and Figure S3d). Increasing the concentration of Mel for loading in the corona led to a slight rise in the overall D_H of SNP//corona (Figure S3d).

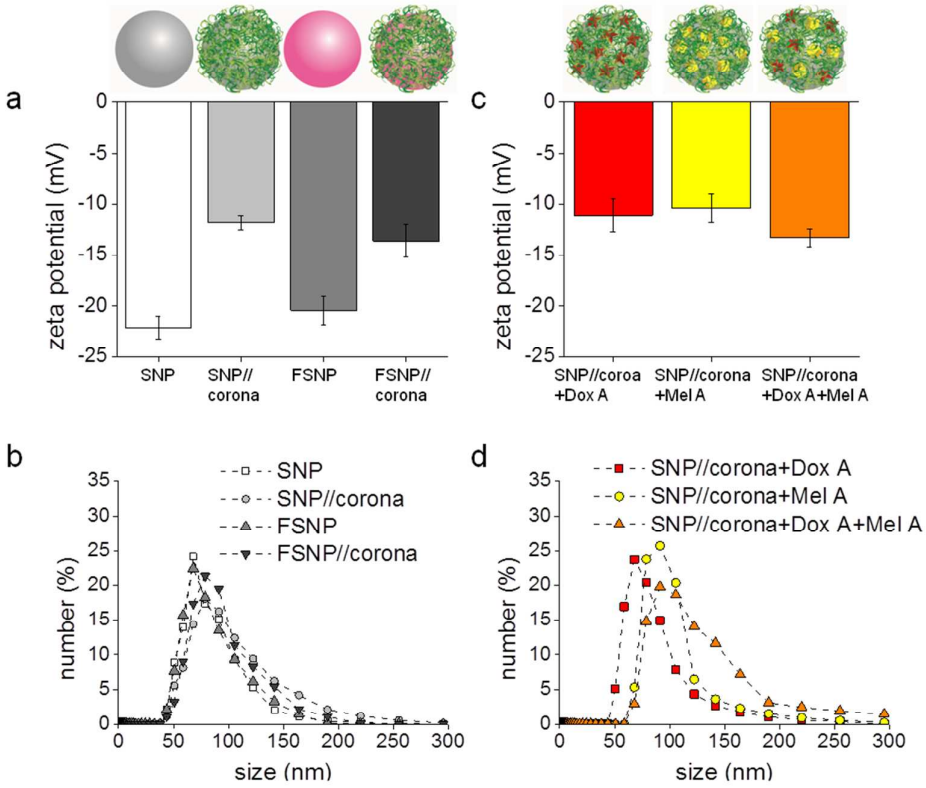

Figure 1. Zeta potential values and size distribution obtained by DLS for SNP and FSNP without or with corona (a, b) and for drug loaded SNP//corona with concentration code A (c, d). Zeta potential data were obtained from triplicate measurements. As defined in **Table 1**, for SNP//corona+Dox A 0.0431 µmol Dox, for SNP//corona+Mel A 1.6669 µmol Mel and for SNP//corona+Dox A+Mel A 0.0431 µmol Dox plus 1.6669 µmol Mel were applied for loading the particle corona with drugs.

The loading efficiency (L.E.) of Dox or Mel in the corona around SNPs was measured after 4 h incubation with FCS at 37 °C (Figure 2a, b and Figure S4a, b). Circa 20-30 % of the initially applied Dox amount was loaded into the corona of SNP//corona+Dox or SNP//corona+Dox+Mel (Figure 2a and Figure S4a). Whereas, the L.E. of Mel in SNP//corona+Mel or SNP//corona+Dox+Mel was slightly lower and accounted after 4 h of incubation to about 10-20 % of the initially applied Mel (Figure 2b and Figure S4b). No significant difference was observed between the L.E. of drugs in corona-covered SNPs loaded with one (Dox or Mel) or both (Dox+Mel) drugs (Figure 2a, b). In addition, the amount of serum proteins adsorbed on each type of drug loaded SNP//corona after 4 h incubation was quantified (Figure 2c and Figure S4c). Similar amounts of adsorbed proteins ranging between 170 and 220 ng/mg SNPs were found for SNP//corona+Dox, SNP//corona+Mel and SNP//corona+Dox+Mel, irrespective of the type or the concentration of the drugs applied.

The time-dependence drug release from the loaded particles into the medium was studied for up to 7 d of incubation at 37 °C at both pH 7.4 and 4.8 (Figure 2d, e and Figure S4d, e). For both types of encapsulated drugs and their combination substantial amounts of drugs (more than 50%) were released from the particles within the first 24 h of incubation (Figure 2d, e and Figure S4d, e), while only little additional drug release was observed during longer incubations for up to 7 d. For Dox, a significantly stronger and faster release from the corona was measured during incubations at pH 4.8 in comparison to the respective pH 7.4 incubations (Figure 2d and Figure S4d), while acidification to pH 4.8 appears not to affect the release of Mel from the particles (Figure 2e and Figure S4e). In addition, the percental drug release appears to be independent from the initial amounts of drugs loaded into the corona as similar results were obtained for each type of SNP//corona+drug irrespective of the three different drug concentrations (Figure S4d, e). Also the amounts of proteins released from the corona-covered particles into the medium after 1, 4 or 7 d of incubation at 37 °C were quantified (Figure 2f and Figure S4f). The obtained values were higher after 4 d of incubation in comparison to that after day 1, but protein desorption was not further increased during longer incubation for 7 d.

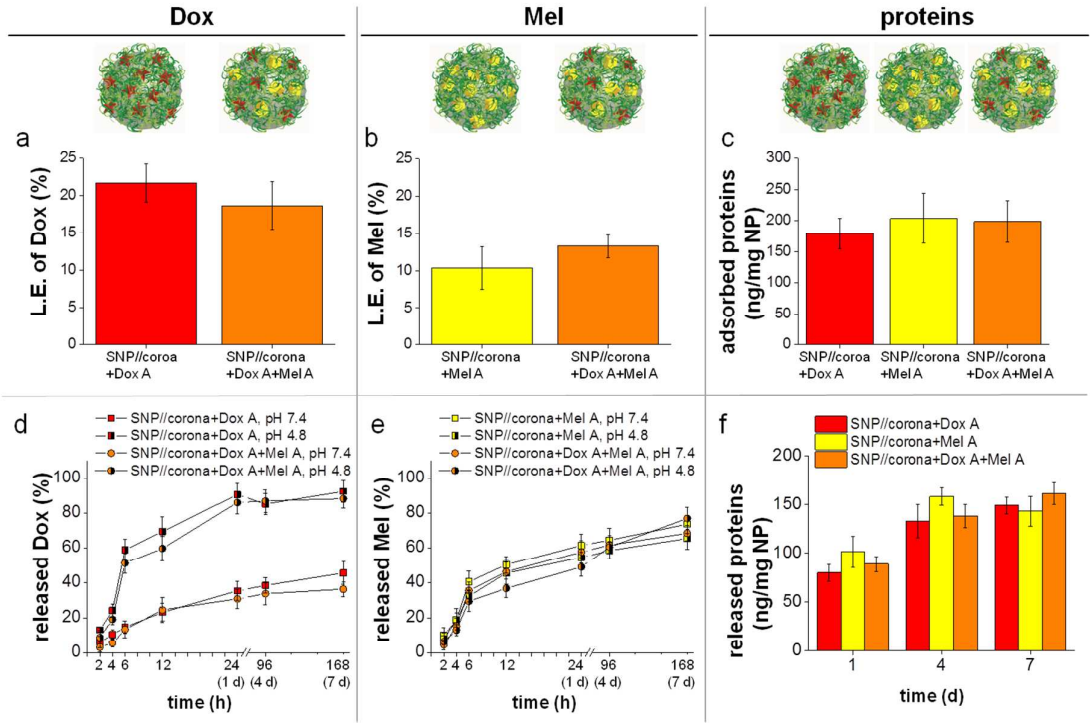

Figure 2. Loading and release of drugs and proteins in and from the corona around SNPs. Loading efficiency (L.E.) of Dox (a) and Mel (b) and adsorbed amount of proteins (c) in the corona around SNPs were determined after 4 h incubation with FCS at 37 °C. Panels d-f show the release of Dox (d), Mel (e) and protein (f) during incubation for up to 7 d. The data of drugs release for each time point

investigated (d, e) are given as percentage of the initially amount loaded for each concentration (a, b). The data were obtained from triplicate measurements.

The effect of drug-free SNP//corona and FSNP//corona on MG-63 cells viability was investigated using water-soluble tetrazolium salt (WST-1) assay and lactate dehydrogenase (LDH) assay (Figure S5a, b). Both assays revealed that exposure to SNP//corona or FSNP//corona did not compromise cellular WST reduction capacity nor induce LDH leakage compared to control cells (incubations without particles or drugs). This demonstrates that the drug-free corona containing SNP nanocarrier did not negatively affect MG-63 cells.

To test for the anti-proliferative potential of drug-loaded SNP//corona as well as of free drugs for MG-63 cells, the WST reduction capacity was determined after 1, 4 or 7 d incubation as indicator for the number of viable cells present.[29, 30] For such WST-1 tests, the free drugs Dox, Mel or Dox+Mel were applied at concentrations equivalent to those present in the applied SNP//corona+drug (Figure 2a, b and Figure S4a, b). The results of such experiments showed clearly that exposure of MG-63 cells to drug-loaded SNP//corona or free drugs lowered the values determined for cellular WST-1 reduction, but with different anti-proliferative potential (Figure 3 and Figure S6). While neither free Mel nor SNP//corona+Mel lowered WST reduction after 1 d of incubation, both treatments significantly lowered WST reduction after 4 d of incubation (Figure 3a, b and Figure S6b). Compared to Mel-containing incubations, the respective treatments with Dox had a stronger potential to lower cell proliferation (Figure 3a, b and Figure S6a). Exposure of cells to SNP//corona+Dox A+Mel A had a stronger anti-proliferative effect than SNPs loaded with only one of the two drugs (SNP//corona+Dox A or SNP//corona+Mel A) (Figure 3b, indicated with +). Similar trend were also observed for the combination of the two free drugs, as Dox A+Mel A was more potent than the single drugs (free Dox A and free Mel A) (Figure 3a, indicated with +). Incubations of cells with drugs delivered from the corona around SNP had either similar or even greater antiproliferative effects than the respective concentration of free drugs (Figure 3a, b). Application of SNP//corona which had been loaded with higher concentrations of the drugs (concentration code C) caused a significantly stronger anti-proliferative effect within 4 d and 7 d than the respective concentration of free drugs (Figure S6a, b, indicated by the symbol §).

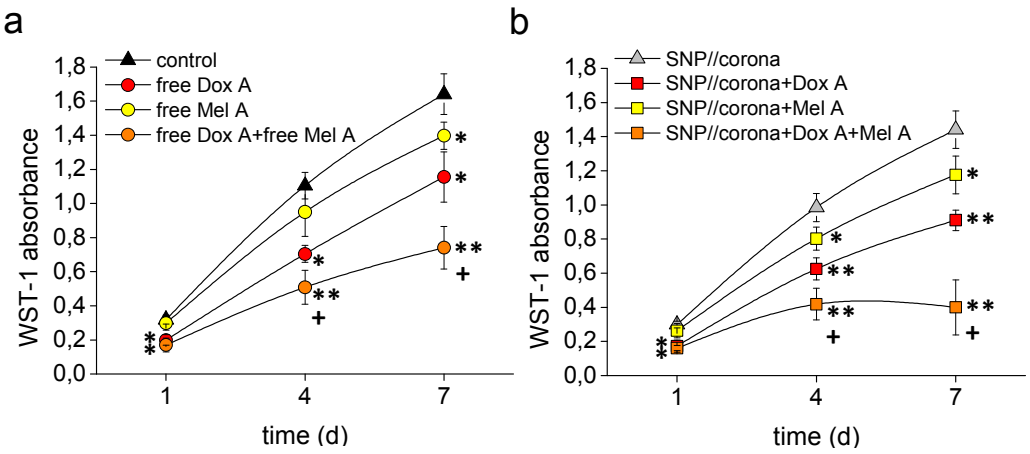

Figure 3. Proliferation of MG-63 cells measured by the WST-1 assay after exposure to free drugs (a) or to SNP//corona+drugs (b) for 1, 4 or 7 d. All data are expressed as mean ± SD of values obtained in three independent experiments. Significant differences in comparison to the respective drug-free controls are indicated by *p<0.05 and **p<0.01. The symbol (+) indicates synergistic effect obtained for a drugs combination compared to the respective incubations with single drugs.

The experiments described above clearly demonstrate the anti-proliferative potential of SNP//corona+drugs (Figure 3). To test whether only the proliferation of MG-63 cells was lowered by exposure to free drugs or SNP//corona+drugs or whether the cells were also damaged by the treatments, the cells were incubated for 1, 4 or 7 d and subsequently stained for fluorescence microscopy and inspected for morphological alterations. None of the conditions applied caused any obvious damage of the cells, although the proliferation of the cells was strongly affected by the presence of free drugs or SNP//corona+drugs. As the results obtained for incubations for 1, 4 or 7 d were almost identical (data not shown), only images obtained after 4 d incubations are shown here (Figure 4). The images of control cells and to blank SNP//corona exposed cells at day 4 are presented in Figure 4a, b. In addition, blank nanocarrier internalization within MG-63 cells was visualized by employment of FSNP//corona (Figure 4c). RBITC-labeled FSNP are visible within the cells with their typical distinct red fluorescence. Representative fluorescence microscopy images of MG-63 cells after exposure to free drugs (Figure 4d-f) and SNP//corona+drugs (Figure 4g-i) at day 4 are presented. The results demonstrated that free Dox with its bright red fluorescence was localized particularly in the MG-63 cell nuclei, whereas, Dox delivered from SNP//corona+Dox or SNP//corona+Dox+Mel was distributed in both cell nuclei and cytoskeletons. As Mel does not feature fluorescence characteristic, it

was not possible to visualize accumulation of free Mel or SNP//corona+Mel in the cells via fluorescence microscopy (Figure 4e, h).

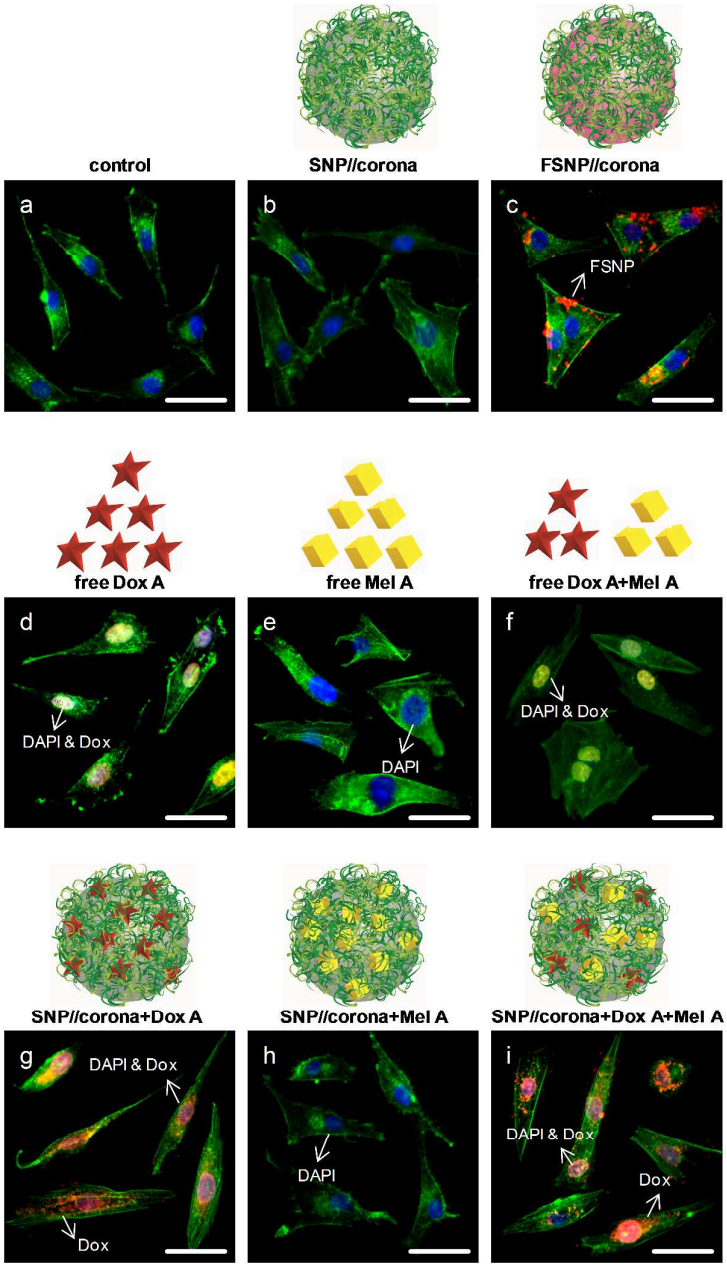

Figure 4. Fluorescence microscopy images of MG-63 cells after 4 d incubation in the absence of drugs and SNPs (control; a), or in the presence of drug-free SNP//corona (b), drug-free FSNP//corona (c), free drugs (d-f) or SNP//corona+drugs (g-i). After the incubation, cell nuclei (blue) and actin cytoskeleton (green) were stained with DAPI and AF488, respectively. The images of cells incubated with free drugs indicated that Dox was present only in cell nuclei (d, f; see overlay of Dox and DAPI), whereas after incubation of the cells with NP//corona+Dox or NP//corona+Dox+Mel Dox fluorescence was found in and outside of nuclei (g,i). Scale bars: 50 μm.

Intracellular localization of SNP//corona+drugs in lysosomes was investigated by fluorescence microscopy after 1, 4 or 7 d exposure to the particles and staining of lysosomes with LysoTracker®. In addition to the blue LysoTracker® staining, the cells were stained for their actin cytoskeleton (green), while the fluorescence of both FSNP and of Dox is presented in red. As the results obtained for incubations for 1, 4 or 7 d were almost identical (data not shown), only images obtained of the MG-63 cells after 4 d of incubation are shown here (Figure 5). Representative fluorescence microscopy images of the MG-63 cells exposed to FSNP//corona (Figure 5a-d), free Dox A (Figure 5e-h), free Dox A+Mel A (Figure 5i-l), SNP//corona+Dox A (Figure 5m-p) and SNP//corona+Dox A+Mel A (Figure 5q-t) are presented. The first column on the left shows merged fluorescence images showing lysosomes (blue), actin cytoskeleton (green) and RBITC-labeled FSNP or Dox (red). The images in the second and third columns show fluorescence images obtained using single blue and red channel originated from LysoTracker® and FSNP or Dox, respectively. The micrographs in the fourth column demonstrate the combination of both blue and red fluorescences. The partial overlapping of LysoTracker® and FSNP or Dox merged to magenta and is indicated by white arrows. The overlay of fluorescences from LysoTracker® and FSNPs (Figure 5d) or Dox (Figure 5p, t) clearly demonstrates their intracellular accumulation of the particles in the endo-lysosomal compartment, while in cells treated with free Dox the Dox fluorescence was found only in the cell nuclei (Figure 5h, l). In contrast, in cells exposed to SNP//corona+Dox A (Figure 5m-p) or SNP//corona+Dox A+Mel A (Figure 5q-t), Dox fluorescence was found in both cell nuclei and lysosomal compartments. As SNP//corona and Mel featured no fluorescence properties, cellular co-localization of such components with LysoTracker® for the respective incubations was not possible. Nevertheless, the fluorescence microscopy images for the respective stainings of control cells and MG-63 cells incubated with SNP//corona, free Mel A or SNP//corona+Mel A are shown in Figure S7.

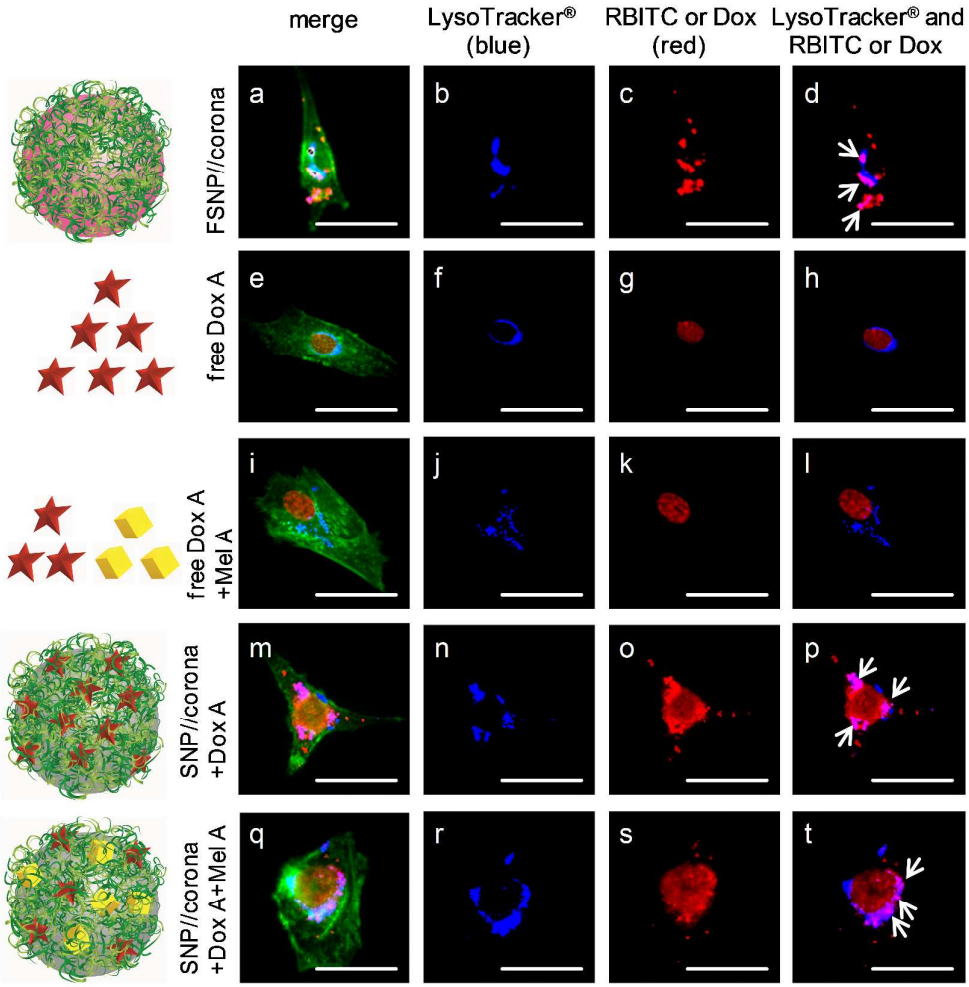

Figure 5. Fluorescence microscopy images of MG-63 cells after 4 d incubation with FSNP//corona (a-d), free Dox A (e-h), free Dox+Mel A (i-l), SNP//corona+Dox A (m-p) or SNP//corona+Dox A+Mel A (q-t). In the first column on the left the merged micrographs of green (actin cytoskeletons), blue (LysoTracker®) and red (RBITC labeled FSNPs and Dox) are presented. The second and third columns show the images in single blue and red channel, respectively. The fourth column indicates the overlay of blue fluorescence of LysoTracker® and red fluorescence originated from FSNPs or Dox, which generates the magenta color indicated by white arrows. Co-localization of the particles and lysosomes was observed using FSNPs (a-d). The images of cells incubated with free drugs showed that Dox was present only in cell nuclei (e-l), whereas after incubation with NP//corona+drugs enhanced Dox fluorescence was found in both nuclei and endo-lysosomal compartments (m-t). Scale bars: 50 µm.

Cellular accumulation of Dox after application of free Dox or SNP//corona+Dox A by MG-63 cells was also quantified by determining the fluorescence of cellular Dox after incubations for 1, 4 or 7 d (Figure 6a and Figure S8a). The intracellular fluorescence of Dox was not affected by the absence or the

presence of Mel. For instance, similar fluorescence signals were obtained from SNP//corona+Dox A and from SNP//corona+Dox A+Mel A for each incubation time (Figure 6a). Correlation between the quantified fluorescence signal originated from intracellular localized Dox and the initial Dox concentration (applied either free or loaded in the corona) was observed (Figure S8a). With increasing incubation time, the Dox fluorescence determined in MG-63 cells was significantly higher after exposure to nanocarrier (SNP//corona+Dox or SNP//corona+Dox+Mel) compared to the respective incubations with free Dox or free Dox+Mel (Figure 6a and Figure S8a, indicated by *).

The quantification of the fluorescence intensity of Dox in the nuclei revealed that for each concentration applied the fluorescence values remained almost constant (Figure 6b), while a concentration-dependent increase in nuclear Dox fluorescence was observed (Figure S8b). After 4 or 7 d of incubation only at the highest applied concentrations of Dox (applied to the cells as SNP//corona+Dox C) a significantly enhanced nuclear Dox fluorescence was observed compared to the respective incubations with identical concentration of free Dox (Figure S8b).

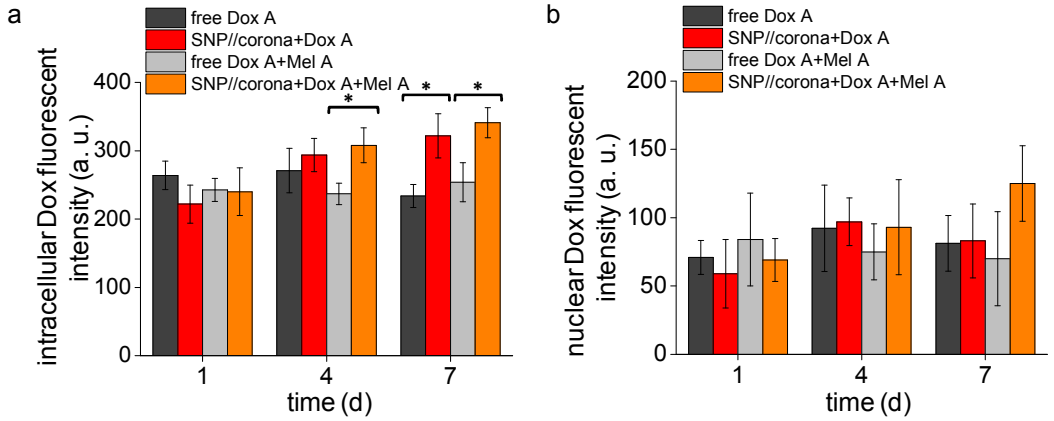

Figure 6. Quantitative comparison of total cellular Dox fluorescence (a) and nuclear Dox fluorescence (b) signal intensity in MG-63 cells that had been incubated for 1, 4 or 7 d with free Dox A, SNP//corona+Dox A, free Dox A+Mel A or SNP//corona+Dox A+Mel A. The data on intracellular Dox fluorescence represent means ± SD of values obtained in three independent experiments. To quantify nuclear Dox internalization for each sampling point, red fluorescence signal of 20 nuclei were analysed by the Zen software. In panel a asterisks (*) indicate significant difference (p<0.05) between the values obtained for SNP//corona+drugs compared to the free drugs applied at the respective concentrations.

4. Discussion

4.1. Characterization of drug nanocarrier

SNPs synthesized via ACSRT were chosen as the substrate for the protein corona formation by incubation in serum supplemented cell culture medium (DMEM+10 % FCS) and for drug loading during corona formation (Scheme 1). The blue-shift of the UV-Vis absorption peak (Figure S2), the drop of zeta potential (Figure 1a) and the slight increase of D_H (Figure 1b) observed for SNPs after incubation with serum show that the surface properties of the bare SNPs altered as a result of being incubated with 10 % FCS. These changes confirm that proteins were adsorbed at SNPs' surface in agreement with the suggested model of the protein corona formation in literature data.[31, 32] Moreover, great stabilization against aggregation is reported for silica particles upon transfer into serum-containing medium.[9] Evidently the protein corona formation is the origin of colloidal stability.[31]

When the particles were dispersed in serum-free DMEM, the zeta potential values depended to some extent on the molecular species at the surface.[9] In contrast, by exposure of SNPs to 10% FCS, their negative surface charges were partially neutralized due to protein adsorption which is consistent with literature data.[33, 34] The zeta potential values of SNPs after corona formation reflect predominately the zeta potential of serum proteins and is mainly derived from serum albumin.[35, 36] Similar negative zeta potential values were determined for the drugs loaded SNP//corona and for the blank unloaded SNP//corona (Figure 1a, c and Figure S3a, c), suggesting that the presence of drugs did not disturb or hinder the corona formation. As loading of SNP//corona with the hydrophilic positively charged Dox[37, 38] or the hydrophobic negatively charged Mel[39, 40] did not result in any significant changes of zeta potential values, one is driven to the conclusion that, the final surface charge is correlated neither with the hydrophobicity nor with the surface charge of the loaded drugs. It suggests that the zeta potential of both blank unloaded and drug-loaded SNP//corona is dominantly defined by the charge and conformation of proteins forming the corona.

For some other types of particles, e.g. 26 nm gold nanorods, the increase of about 290 nm is reported as a consequence of incubation in serum, suggesting that the corona is a large agglomerate containing several particles.[14] However, for many other particles such as different sized silica or functionalized polystyrene, the size distribution of particle-protein complexes is only partially shifted with respect to that of the bare NPs [31, 32] indicating that a protein layer is formed on the particles. In addition, it is reported that the corona thickness becomes smaller at higher plasma concentrations.[32]

Our DLS measurement of the size results in a typical monomodal distribution for both bare and protein-coated SNPs, with the average hydrodynamic diameter being about 10 nm larger for SNP//corona or FSNP//corona than SNP or FSNP, respectively (Figure 1b). At the serum concentration applied for covering SNPs with proteins in our study, this small increase in the corresponding D_H can be attributed to the thickness of the protein coating. Moreover, loading of Dox in the corona led only to slight changes in the overall D_H of SNP//corona (Figure 1d and Figure S3b), whereas D_H was found increased after incorporation of hydrophobic, negatively charged Mel into the corona, either alone or in combination with Dox (Figure 1d and Figure S3d). This suggests that Mel-loading might form SNP-protein cluster. Constant and gradual changes in the overall size of drug loaded SNP//corona with increasing drugs concentration indicated that loading of both drugs in the corona was proportional to their initially applied amounts. The difference in the sizes of Dox- and Mel-loaded SNP//corona suggest that these drugs interact with different serum proteins during corona formation.

The obtained data on L.E. of the drugs indicated that the corona around SNPs incorporated both hydrophilic and hydrophobic drug molecules during simultaneous incubation with serum. The presence of different protein and corona structure can provide large volume “containers” for drug payload. Indeed, hydrophilic and hydrophobic sites of proteins enhance loading capacity of the corona to host both types of therapeutics.[16] Quantification of drugs payload showed that Dox could be loaded into the forming corona with a slightly higher efficiency than Mel (Figure 2a, b and Figure S4a, b). This confirms a given specificity of the interactions between serum proteins and each drug, most likely due to the difference in the charge and the hydrophilicity of the two drugs. Typically hydrophobic/hydrophilic and electrostatic interactions are known to be involved in for the corona assembly [41-43] and also in the drug loading.[14] Although both Dox and Mel have hydrophilic and hydrophobic groups which may interact with respective sites of serum proteins, Dox is dominantly hydrophilic,[37] while Mel is more hydrophobic.[40] We believe that the hydrophilicity and the positive charge of Dox will facilitate the loading of this drug into a corona containing negatively charged serum proteins. In contrast, hydrophobicity and electrostatic repulsion between the negative Mel and serum proteins may limit Mel binding to SNP//corona, thereby leading to a lower L.E.

Notably, the percental L.E. of Dox and Mel into SNP//corona did not change significantly by the variation of the initial drug amounts (Figure S4a, b). These results demonstrate that the loading of both drugs increased almost proportional to the initial amount of drugs applied, suggesting that the maximal

loading capacity of the corona around SNPs can be higher than the concentrations chosen for each drug.

Quantification of the proteins adsorption on SNPs showed similar values for all prepared SNP//corona+drugs (Figure 2c and Figure S4c), suggesting that the amount of adsorbed proteins was affected neither by the type nor by the concentration of the drugs applied. It is worth emphasising here that high variability in the drugs L.E. (Figure 2a, b and Figure S4a, b) as well as in the amount of the adsorbed proteins (Figure 2c and Figure S4c) is likely to be due to the complex and random nature of the corona formation involving nonspecific interactions between multiple protein species.[14]

Results obtained from drug release studies clearly demonstrated that drugs are released over time from the corona around SNPs and that during incubations for up to 7 d most of the initially loaded Dox or Mel was found in the supernatant (Figure 2d, e and Figure S4d, e). The non-covalent nature of the drug loading is most likely responsible for making the drugs available for release into the medium.[16] For Dox, release from the particle corona was significantly higher and faster at pH 4.8 compared to the respective pH 7.4 condition (Figure 2d and Figure S4d), suggesting that after cellular internalization of SNP//corona+Dox the drug would be rapidly liberated from the particle corona in the acidic lysosomal compartment which should increase the efficiency of such particles to prevent cell proliferation. The increased water solubility of Dox at lower pH values via a proton sensitive mechanism [16, 28, 44] may lead to its higher release. At both pH values investigated, almost maximal Dox release was observed after 1 d of incubation and the amount of Dox released did not change considerably during longer incubation periods. Compared to Dox, release of Mel from the corona was slower and the Mel release was not stimulated by acidic pH. Potential reasons for the slower release of Mel from the particle corona in comparison to Dox could be a stronger binding of Mel in the hydrophobic regions of the corona or its low water solubility.[40]

In a biological environment, NP–biomolecule complexes are composed of the core NP surrounded by a strongly associated proteins and an outer collection of weakly interacting biomolecules.[3, 45, 46] These two protein layers are completely different in terms of their timescales. The stabilizing coating of the bare surface of NPs, named the "hard" corona, exchanges often over several hours.[31, 42, 47] Whereas, for the outer protein coating, "soft" corona, a lifetime of seconds or less is expected.[47] In our procedure, the purification of the SNP//corona from unbound and loosely associated proteins by the centrifugation, washing and resuspending provides a robust protein coating on the SNPs.[31] Therefore, we hypothesize that the drugs were loaded in a sufficiently stable, durable and long-lived protein

coating. In fact, a protein layer residing longer than the characteristic timescale of biological processes may be relevant to retain and delivery therapeutic molecules. As endocytosis of NPs across the cell membrane occurs within minutes,[48] we assume that the protein coating containing drugs stay on the SNPs' surface at least this long to be taken up and processed by the endocytic machinery.

It is worth mentioning that although the relatively immobile protein layer binds tightly on the NPs' surface and maintains its primary structural properties over many hours, it is not completely irreversible.[31, 49, 50] Indeed, via dynamical exchange processes, proteins can adsorb and desorb to the surface of NPs or they can displace other proteins.[42, 49] Therefore, the corona evolution, protein association with/dissociation from SNPs over time, accompanies the release of payloads from the corona into cells. Remarkably, the time dependency of protein release was observed, irrespective of the type or the concentration of the loaded drug (Figure 2f and Figure S4f). For the conditions applied here it cannot be excluded that a part of the drug release from the particles could be a consequence of protein corona evolution.

4.2. Cell culture experiments

The WST-1 assay was used to determine MG-63 cell proliferation and therefore anti-cancer efficiencies of our nanocarries loaded with different drug concentrations (Figure 2a, b and Figure S4a, b). Since the particle cytotoxicity has an essential impact on their applications in the drug delivery field, preliminary biocompatibility evaluations are necessary.[51] Therefore, it was first confirmed by using both WST-1 and LDH assays that the unloaded SNP//corona were not cytotoxic and had no anti-proliferative potential (Figure S5). In contrast, free and corona-loaded therapeutics severely decreased the proliferation of MG-63 cells (Figure 3 and Figure S6). As the blank nanocarrier did not affect cell proliferation (Figure S5), any decrease of the cell proliferation was likely attributable to the released drugs from the corona and their successful delivery in the cells (Figure 3b and Figure S6a, b).

Although the number of cells per well was lowered after incubation with free drugs or with the different types of SNP//corona+drugs, which is demonstrated by the low WST reduction capacity observed for these conditions (Figure 3 and Figure S6), no obvious cell damage or severely altered cell morphology compared to control incubations were observed (Figure 4). This observation strongly suggests that the drugs applied have under the conditions used predominantely anti-proliferative functions, which is consistent with literature data.[23, 25, 26]

Time and concentration dependencies were observed for the anti-proliferative effects of free and SNP//corona-containing drugs. While, Mel did not affect proliferation before day 4, which is consistent to the report of Wolfesberger et al.,[25] Dox inhibited cell growth of MG-63 cell already within 1 d of incubation. Notably, the highest possible therapeutic benefit of both drugs was observed after 4 d incubation (Figure 3 and Figure S6). Although release studies (Figure 2d and Figure S4d) revealed that specifically the highest possible Dox payload was released from the corona at day 1, both free and in the corona loaded Dox needed apparently more time to prevent proliferation even at the highest concentration applied (Figure 3 and Figure S6a).

At the highest concentrations applied, the SNP//corona+drugs drastically decreased the cell proliferation and showed an even higher anti-proliferative potential than the free drugs (symbol (&) in Figure S6a, b). This is likely due to the higher cellular concentration of the drugs in cells which were exposed to SNP//corona +drugs compared to cells treated with free drugs, as quantified at least for Dox (Figure 6 and Figure S8). Similar results have been reported for other types of nanocarriers applied for drug delivery, which could contribute to the overall decrease in the cell viability and higher therapeutic efficiency compared to the free drugs.[16, 52, 53] As greater amounts of drugs could be intracellulary delivered by using the nanocarriers, the cells are more vulnerable to the anti-proliferation effects of the loaded drugs.[54, 55] A possible explanation for such findings could be the phenomenon of multidrug resistance (MDR) of cancer cells, which is usually mediated by the overexpression of P-glycoprotein (P-gp) and other membrane transporters.[28, 56] As such drug efflux transporters reduce the cellular concentration of a broad spectrum of cytotoxic anticancer drugs in cancer cells,[54, 55, 57] the cellular delivery of therapeutics using nanocarriers via endocytotic pathways may avoid export by by-passing the P-gp pump and other drug transporters.[51] Indeed, our results confirm that Dox delivery using SNP//corona at least for the highest concentration applied, increased total intracellular Dox concentration (Figure 6a and Figure S8a) and nuclear Dox accumulation (Figure 6b and Figure S8b) which is accompanied by an enhanced anti-proliferation effect (Figure 3 and Figure S6) compared to free Dox. MDR of MG-63 cells was found to be stronger at higher drug dosages. The dependency of osteosarcomas' MDR-responses on the drug concentration applied for the therapy needs to be studied in more details.

Mel is a cycloxygenase-2 (COX-2) inhibitor, which has been shown to exert inhibitory effects on different types of malignant tumors.[58, 59] Potential clinical applications for COX-2 inhibitors have been suggested, as such compounds enhance the therapeutic effects of other anti-cancer agents, when

they are used in combination.[60, 61] The synergy between free Mel and chemotherapeutics such as Dox has been previously evaluated, using different osteosarcoma cell lines.[25, 26] Our results clearly show that in the presence of both Mel and Dox loaded in SNP//corona synergistically enhanced the anti-proliferation effect of Dox (Figure 3b). Some reports suggested that the synergistic effects, seen with COX-2 inhibitors and Dox, might depend on the enhancement of apoptosis via different mechanisms.[26, 62] Other groups have reported that the observed synergy is the result of an inhibition of MDR gene expression leading to a higher intracellular accumulation of Dox.[63, 64] However, we observed no evidence for increased Dox internalization after exposure in combination with Mel, as at all incubation times studied (1, 4 or 7 d) intracellular as well as nuclear Dox fluorescence intensities of SNP//corona+Dox A and SNP//corona+Dox A+Mel A were similar (Figure 6a, b). This finding might weaken the idea that presence of Mel could lower MDR-mediated Dox export in osteosarcoma and suggests that other mechanisms could be responsible for the achieved synergistic anti-proliferative outcome.

The cellular internalization of the drug loaded SNP//corona was studied *in vitro* by their application to MG-63 cells. Fluorescence of FSNP provided the visualization of the intracellular distribution of the particles close to the cytoskeleton. Fluorescence microscopy analysis (Figure 4c) showed that FSNP//corona were found distributed inhomogeneously in the cells, mostly around the nucleus which is in agreement with the report of Al-Rawi et al..[11] The presence of Dox in the cells was demonstrated by its distinct red fluorescence, as no such emission was observed for untreated MG-63 cells (Figure 4a) or cells exposed to the unloaded SNP//corona (Figure 4b). Since no nuclear uptake of FSN//corona was observed (Figure 4c), it is likely that the red emitting fluorescence of Dox in the nuclei was due to the released Dox from the loaded SNP//corona (Figure 4g, i). This result implies that Dox is carried by the particles into the cells and released inside the MG-63 cells. Remarkably, studying the intracellular localization of Dox after exposure of cells to free Dox, either alone or in combination with Mel, revealed that Dox was only present in substantial amounts in the cell nucleus (Figure 4d, f), while Dox release from the single or dual loaded SNP//corona resulted in fluorescence signals both in nucleus and close to the cytoskeleton (Figure 4g, i). These data not only demonstrated that SNP//corona serves as efficient vehicle to transport Dox into MG-63 cell, but also that the particles are internalized and distributed by cellular pathways that differ from those used for free Dox. Free Dox has been shown to enter cell via a passive diffusion mechanism,[65] while SNP//corona are likely to be taken up into MG-63 via an endocytic pathway to become directed into the lysosomal compartment, as

confirmed by straining with LysoTracker® (Figure 5). As Dox release from the corona of SNP//corona-Dox was accelerated at pH 4.8 (Figure 2d and Figure S4d), intracellular trafficking of such particles into the acidic lysosomal compartment is likely to contribute to efficient intracellular drug release from the particles, which will support the anti-proliferative potential of Dox-loaded SNP//corona.

As it is known that the protein corona around NPs evolves with time,[42] also evidences exist that proteins associated with internalized particles can be degraded intracellularly.[66] For particles internalized in mammalian cells, one may expect partial digestion of the corona in endosomal compartments[67] and in extreme cases, e.g., following particle localization in lysosomes, even entire corona removal is possible.[67, 68] Endosytosis uptake of NPs involves transport of the NPs to endocytic vesicles,[69] in which proteolytic enzymes, known as proteinases or proteases, are present that digest the proteins.[68, 70] Degradation of the protein coatings upon enzymatic digestion might be harnessed for drug delivery applications.[70] For instance, the loaded drugs in NPs can be subsequently released in a sustained manner exclusively upon enzymatic digestion of the protein corona in the presence of proteolytic enzymes.[68] Therefore, besides the acidic pH values of lysosomal compartments, which accelerate Dox release, enzymatic degradation of the protein corona in lysosomes can also enhance the release of therapeutics. It suggests that proteolytic degradation of the corona around SNPs might serve as a trigger to control the release of the encapsulated Dox and Mel at a specific local environment of osteosarcomas.

To apply NPs for therapeutic purposes, many active targeting strategies have been suggested. One approach to obtain a high targeting yield is to functionalize the NPs' surface with targeting agents such as antibodies or aptamers that enhance NP binding to receptors on the target cells and facilitate cellular uptake of NPs.[71, 72] Despite the remarkable potential, these strategies have met with limited success in practice. In fact, where targeting moieties are grafted onto NPs' surface, they may not retain their function as a result of poor orientation and structural or conformational disruption.[73] Moreover, the corona formation may reduce the targeting capability of surface engineered NPs by screening the active sites of the targeting ligands.[73, 74] A second approach for targeting involves exploitation of the protein corona itself, by understanding which proteins effectively deliver particles to which location.[73] To transfer the remarkable possibilities of the protein corona around SNPs for drug loading and release into therapeutical applications, more detailed and dedicated investigations on the targeting capability of SNP-protein complexes are needed.

5. Conclusions

We developed a novel SNPs that could be used as nanocarrier for efficient dual anti-cancer drug delivery by exploiting the protein corona formed by serum proteins. Corona conjugated SNPs could be efficiently loaded with both hydrophilic and hydrophobic anticancer drugs (alone or in combination) in a specific and controllable manner. We found that loaded drugs could be released and delivered to cancer cells, and their effect was even enhanced compared to those of the free drugs. The highest anti-proliferative efficiency was obtained by the combination of the two anticancer drugs doxorubicin and meloxicam, suggesting a synergetic therapeutic effect of these two drugs. The feasibility of the simultaneous corona formation and drug encapsulation, the advantage of loading both hydrophilic and hydrophobic drugs in one particle as well as the release of the potent therapeutic molecules from the internalized nanocarriers in cancer cells make the protein corona around SNPs a promising and versatile structure to facilitate drug delivery and therapeutic purposes.

Supporting Information

Supporting Information is available from the *Wiley Online Library* or from the author.

Acknowledgements

We greatly thank Dr. Thorsten Mehrtenz (Solid State Physics, University Bremen) for TEM analysis. This work was supported by the European Research Council within the SIRG Project “BiocerEng” Project No. 205509.

References

[1. M. Mahmoudi, I. Lynch, M. Ejtehadi, M. Monopoli, F. Bombelli and S. Laurent, *Chem. Rev.* , 2011, **111**, 5610–5637.
2. A. Nel, L. Mädler, D. Velegol, T. Xia, E. Hoek, P. Somasundaran, F. Klaessig, V. Castranova and M. Thompson, *Nature Materials* 2009, **8**, 543-557.
3. T. Cedervall, I. Lynch, S. Lindman, T. Berggård, E. Thulin, H. Nilsson, K. Dawson and S. Linse, *PNAS* 2007, **104**, 2050–2055.
4. M. Lundqvist, J. Stigler, G. Elia, I. Lynch, T. Cedervall and K. Dawson, *PNAS* 2008, **105**, 14265–14270.
5. S. Park and K. Hamad-Schifferli, *ACS Nano*, 2010, **4**, 2555–2560.
6. D. Mahl, C. Greulich, W. Meyer-Zaika, M. Köller and M. Epple, *J. Mater. Chem.*, 2010, **20**, 6176–6181.
7. J. Gebauer, M. Malissek, S. Simon, S. Knauer, M. Maskos, R. Stauber, W. Peukert and L. Treuel, *Langmuir* 2012, **28**, 9673−9679.
8. A. Albanese and W. C. W. Chan, *ACS Nano*, 2011, **5**, 5478–5489.

9. S. Shahabi, L. Treccani, R. Dringen and K. Rezwan, *ACS Appl. Mater. Interfaces* 2015, **7**, 13821−13833.
10. Y. Qiu, Y. Liu, L. Wang, L. Xu, R. Bai, Y. Ji, X. Wu, Y. Zhao, Y. Li and C. Chen, *Biomaterials*, 2010, **31**, 7606–7619.
11. M. Al-Rawi, S. Diabate´ and C. Weiss, *Arch Toxicol*, 2011, **85**, 813-826.
12. K. Prapainop, D. P. Witter and J. P. Wentworth, *JACS*, 2012, **134**, 4100−4103.
13. C. Ge, J. Du, L. Zhao, L. Wang, Y. Liu, D. Li, Y. Yang, R. Zhou, Y. Zhao, Z. Chai and C. Chen, *PNAS*, 2011, **108**, 16968–16973
14. J. C. Y. Kah, J. Chen, A. Zubieta and K. Hamad-Schifferli, *ACS Nano*, 2012, **6**, 6730–6740.
15. A. Cifuentes-Rius, H. de Puig, J. C. Y. Kah, S. Borros and K. Hamad-Schifferli, *ACS Nano*, 2013, **7**, 10066–10074.
16. R. Khandelia, A. Jaiswal, S. S. Ghosh and A. Chattopadhyay, *Small*, 2013, **9**, 3494–3505.
17. S. Shahabi, L. Treccani and K. Rezwan, *J Nanopart Res*, 2015, **17**, 1-15.
18. X. Gao, J. He, L. Deng and H. Cao, *Optical Materials*, 2009, **31**, 1715–1719.
19. J. Peng, X. He, K. Wang, W. Tan, Y. Wang and Y. Liu, *Anal Bioanal Chem* 2007, **388**, 645–654.
20. R. Kumar, I. Roy, T. Ohulchanskky, L. Vathy, E. Bergey, M. Sajjad and P. Prasad, *ACS Nano*, 2010, **4**, 699–708.
21. S. Santra, P. Zhang, K. Wang, R. Tapec and W. Tan, *Anal. Chem.*, 2001, **73**, 4988-4993.
22. J. Lee, Y. Jun, S. Yeon, J. Shin and J. Cheon, *Angew. Chem.*, 2006, **118**, 8340–8342.
23. B. Wolfesberger, I. Walter, C. Hoelzl, J. G. Thalhammer and M. Egerbacher, *Research in Veterinary Science* 2006, **80**, 308–316.
24. H. Ganjavi, M. Gee, A. Narendran, N. Parkinson, M. Krishnamoorthy, M. Freedman and D. Malkin, *Cancer Gene Therapy* 2006, **13**, 415–419.
25. B. Wolfesberger, C. Hoelzl, I. Walter, G. A. Reider, G. Fertl, J. G. Thalhammer, M. Skalicky and M. Egerbacher, *J. vet. Pharmacol. Therap.*, 2006, **29**, 15-23.
26. T. Naruse, Y. Nishida and N. Ishiguro, *Biomedicine & Pharmacotherapy*, 2007, **61**, 338-346.
27. M. Holthaus, J. Stolle, L. Treccani and K. Rezwan, *Acta Biomaterialia* 2012, **8**, 394–403.
28. H. Meng, M. Liong, T. Xia, Z. Li, Z. Ji, J. Zink and A. Nel, *ACS Nano*, 2010, **4**, 539–4550.
29. M. Dews, A. Homayouni, D. Yu, D. Murphy, C. Sevignani, E. Wentzel, E. Furth, W. Lee, G. Enders, J. Mendell and A. Thomas-Tikhonenko, *Nature genetics*, 2006, **38**, 1060-1066.
30. K. Kozaki, I. Imoto, S. Mogi, K. Omura and J. Inazawa, *Cancer Research* 2008, **68**.
31. D. Walczyk, F. Bombelli, M. Monopoli, I. Lynch and K. Dawson, *J. AM. CHEM. SOC.*, 2010, **132**, 5761–5768.
32. M. Monopoli, D. Walczyk, A. Campbell, G. Elia, I. Lynch, F. Bombelli and K. Dawson, *J. Am. Chem. Soc.* , 2011, **133**, 2525–2534.
33. D. Guarnieri, M. Malvindi, V. Belli, P. Pompa and P. Netti, *J Nanopart Res* 2014, **16**, 1-14.
34. Y. Yan, K. Gause, M. Kamphuis, C. Ang, N. O'Brien-Simpson, J. Lenzo, E. Reynolds, E. Nice and F. Caruso, *ACS Nano*, 2013, **7**, 10960–10970.
35. M. Horie, H. Kato and H. Iwahashi, *Arch Toxicol* 2013, **87**, 771–781.
36. C. Fleischer and C. Payne, *J. Phys. Chem. B* 2012, **116**, 8901−8907.
37. H. Wang, Y. Zhao, Y. Wu, Y. Hu, K. Nan, G. Nie and H. Chen, *Biomaterials* 2011, **32**, 8281-8290.
38. K. Janes, M. Fresneau, A. Marazuela, A. Fabra and M. Alonso, *Journal of Controlled Release* 2001, **73**, 255–267.
39. N. Seedher and S. Bhatia, *Journal of Pharmaceutical and Biomedical Analysis* 2005, **39**, 257–262.
40. S. Sharma and A. Pawar, *International Journal of Pharmaceutics* 2006, **313**, 150–158.
41. I. Lynch and K. Dawson, *Nano Today*, 2008, **3**, 40-47.
42. E. Casals, T. Pfaller, A. Duschl, G. J. Oostingh and V. Puntes, *ACS Nano*, 2010, **4**, 3623–3632.
43. P. Aggarwal, J. Hall, C. McLeland, M. Dobrovolskaia and S. McNeil, *Advanced Drug Delivery Reviews* 2009, **61**, 428–437.
44. H. Yoo and T. Park, *Journal of Controlled Release* 2001, **70**, 63-70.
45. I. Lynch, A. Salvati and K. Dawson, *Nature Nanotechnology*, 2009, **4** 546–547.

46. I. Lynch, T. Cedervall, M. Lundqvist, C. Cabaleiro-Lago, S. Linse and K. Dawson, *Advances in Colloid and Interface Science* 2007, **134–135**, 167–174.
47. S. Milani, F. Bombelli, A. Pitek, K. Dawson and J. Rädler, *ACS Nano*, 2012, **6**, 2532–2541.
48. A. Salvati, C. Åberg, T. dos Santos, J. Varela, P. Pinto, I. Lynch and K. Dawson, *Nanomed.: Nanotechnol., Biol. Med.*, 2011, **7**, 818–826.
49. M. Monopoli, C. Åberg, A. Salvati and K. Dawson, *Nature Nanotechnology*, 2012, **7**, 779-786.
50. P. del Pino, B. Pelaz, Q. Zhang, P. Maffre, G. Nienhaus and W. Parak, *Mater. Horiz.*, 2014, **1**, 301–313.
51. C. Manaspon, K. Viravaidya-Pasuwat and N. Pimpha, *Hindawi Publishing Corporation, Journal of Nanomaterials*, 2012, 1-11.
52. X. Zhang, H. Chibli, R. Mielke and J. Nadeau, *Bioconjugate Chem.* , 2011, **22**, 235–243.
53. K. Upadhyay, A. Bhatt d, A. Mishra, B. Dwarakanath, S. Jain, C. Schatz, J. Le Meins, A. Farooque, G. Chandraiah, A. Jain, A. Misra and S. Lecommandoux, *Biomaterials* 2010, **31**, 2882–2892.
54. H. L. Wong, A. M. Rauth, R. Bendayan, J. L. Manias, M. Ramaswamy, Z. Liu, S. Z. Erhan and X. Y. Wu, *Pharmaceutical Research*, 2006, **23**, 1574-1585.
55. H. S. Yoo and T. G. Park, *Journal of Controlled Release*, 2004, **96**, 273-283.
56. M. M. Gottesman, *Annu. Rev. Med.*, 2002, **53**, 615–627.
57. H. Coley, P. Twentyman and P. Workman, *Bmchemwal Phormcology*, 1993, **46**, 1317-1326.
58. C. Montejo, E. Barcia, S. Negro and A. Fernández-Carballido, *International Journal of Pharmaceutics* 2010, **387**, 223–229.
59. T. Naruse, Y. Nishida, K. Hosono and N. Ishiguro, *Carcinogenesis*, 2006, **27**, 584–592.
60. M. H. Hassan, H. A. El-Beshbishy, H. Aly, S. M. Attia, S. A. Bahashwan and M. M. Ghobara, *Cancer Chemother Pharmacol*, 2014, **74**, 559–569.
61. J. Lin, P. Hsiao, T. H. Chiu and J. Chao, *Biochemical Pharmacology* 2005, **70**, 658–667.
62. A. Haynes, M. Shaik, A. Chatterjee and M. Singh, *Pharmaceutical Research*, 2003, **20**, 1485-1495.
63. H. Kang, E. Lee, H. Pyo and S. Lim, *Mol Cancer Ther* 2005, **4**, 1358-1363.
64. M. Zatelli, A. Luchin, D. Piccin, F. Tagliati, A. Bottoni, C. Vignali, M. Bondanelli and E. degli Uberti, *The Journal of Clinical Endocrinology & Metabolism* 2005, **90**, 5754–5760.
65. X. Xiong, A. Mahmud, H. Uludağ and A. Lavasanifar, *Pharmaceutical Research*, 2008, **25**.
66. P. Rivera-Gil, S. De Koker, B. De Geest and W. Parak, *Nano Lett.*, 2009, **9**, 4398-4402.
67. V. Se´e, P. Free, Y. Cesbron, P. Nativo, U. Shaheen, D. Rigden, D. Spiller, D. Fernig, M. White, I. Prior, M. Brust, B. Lounis and R. Le´vy, *ACS Nano*, **3**, 2461–2468.
68. M. Chanana, P. Rivera-Gil, M. Correa-Duarte, L. Liz-Marz and W. Parak, *Angew. Chem. Int. Ed.*, 2013, **52**, 4179 –4183.
69. T. Iversen, T. Skotland and K. Sandvig, *Nano Today*, 2011, **6**, 176-185.
70. J. Wang, Y. Yue, G. Chen and J. Xia, *Soft Matter*, 2011, **7**, 7217-7222.
71. X. Gao, Y. Cui, R. Levenson, L. Chung and S. Nie, *Nature Biotechnology*, 2004, **22** 969-976.
72. O. Farokhzad, S. Jon, A. Khademhosseini, T. Tran, D. LaVan and R. Langer, *Cancer Research*, 2004, **64**, 7668–7672.
73. E. Mahon, A. Salvati, F. Bombelli, I. Lynch and K. Dawson, *Journal of Controlled Release* 2012, **161**, 164–174.
74. A. Salvati, A. Pitek, M. Monopoli, K. Prapainop, F. Bombelli, D. Hristov, P. Kelly, C. Åberg, E. Mahon and K. Dawson, *Nature Nanotechnology*, 2013, **8**, 137-143.